Centrifugal Pump Model of the DLR Thermofluid Stream Library

Raphael Gebhart[1] Martin Düsing[2] Niels Weber[1] Franciscus L. J. van der Linden[1]

[1]Institute of System Architectures in Aeronautics, German Aerospace Center, Münchener Strasse 20, 82234 Weßling, Germany, {raphael.gebhart,franciscus.vanderlinden,niels.weber}@dlr.de

[2]HELLA GmbH & Co. KGaA, Beckumer Str. 130, 59552 Lippstadt, Germany, martin.duesing@forvia.com

Abstract

Modeling pumps in 1D flows in Modelica is not new. In this paper a new approach is presented that can be used for general centrifugal pumps as well as centrifugal pumps based on measurement data for the DLR Thermofluid Stream (TFS) Library. The presented model uses affinity laws for good scaling. This approach allows to predict the pump behavior also for pumps where no measurement data exist based on data from similar pumps. The models are designed with focus on numerically robustness and focus on normal pump operation. They avoid nonlinear equation systems and can be initialized at zero mass flow rate and/or zero speed. Furthermore care has been taken that extrapolation of the pump data outside the data range is robust without interpolation artifacts. A pump surge example demonstrates that the TFS can handle instationary abnormal pump behavior like surge limit cycles by default without any further modifications needed.

Keywords: Centrifugal Pump; Hydraulic Transients; Thermal Modeling; Thermofluid Stream; TFS

1 Introduction

The pump models available in the Thermofluid Stream (TFS) Library (Zimmer 2020; Zimmer, Meißner, and Weber 2022) have been used for simple modeling tasks. However, in order to create more realistic pumps or pumps based on real measurement data, we have found that current models do not meet all the requirements needed by industry. Therefore, new pump models have been developed that are more realistic. These models are in contrast to the models from Modelica.Fluid, since they avoid division by zero. Furthermore they avoid using polynomials of high degree for interpolation, which can cause oscillation at the edges of the interpolation interval known as *Runge's phenomenon*, see (Trefethen 2019). There exists extensive literature on pump modeling, well known german-language books are e.g. (Gülich 2010) or (Sigloch 2013), and english-language books are e.g. (Stepanoff 1957) or (Karassik et al. 2007). Furthermore it might be worth mentioning (Chaudhry 2014) focusing on hydraulic transients. In Modelica pump models are part of fluid libraries as Modelica.Fluid (Casella et al. 2006), the Buildings Library (Wetter et al. 2014) or TIL Library (Richter 2008). Modelica.Fluid uses polynomial interpolation for head characteristic and either fixed efficiency or quadratic power characteristic. For the Buildings Library one can use spline interpolation of measurement data. The model incorporates several numerical workarounds to avoid singularities and ensure a unique solution (Wetter 2013). Alternatively a method based on the Euler Number can be used that requires only reference values at the point of best efficiency as inputs (Fu, Blum, and Wetter 2023). The TIL Library uses a quadratic head characteristic $h \sim \dot{V}|\dot{V}|$ that has an inflection point at zero flow and uses an empirical relation for the loss power.

First, subsection 2.1 introduces the centrifugal pump model. Subsequently in subsection 2.2 measurements of a sample development pump from the automotive supplier HELLA GmbH & Co. KGaA are used, to validate the pump model, see an example in Figure 1. These pumps, which are developed in several power classes from 80 W to 400 W, are used in battery electric cars to cool and heat several components (e.g. battery, electrical machine, cabin). In most cooling systems the pumps are integrated into a Coolant Control Hub (CCH) together with valves. The fluid used in these systems are mixtures of water and glyocol. In addition, the models have been validated against data from pumps available in the Modelica Buildings library (Wetter et al. 2014). In subsection 2.3 it is shown that centrifugal pump characteristics have great similarities. Hence realistic pump characteristics can be set up with minimum knowledge. Furthermore in section 3, a pump surge example demonstrates that the TFS can handle instationary abnormal pump behavior like surge limit cycles by default without any further modifica-

tions needed and without any numerical modifications of the pump characteristics necessary.

Figure 1. Sample automotive development pump (copyright HELLA GmbH & Co. KGaA).

2 Centrifugal pump model

2.1 Basic equations

The centrifugal pump model is based on affinity laws that govern the scaling behavior of head $h \sim \omega^2$, discharge $\dot{V} \sim \omega$, and power $P \sim \rho\omega^3$ with respect to speed ω and fluid density ρ. These relationships, commonly referred to as homologous relationships, are detailed in any textbook on pumps e.g. (Stepanoff 1957; Karassik et al. 2007; Gülich 2010; Sigloch 2013). The model targets normal pump operating conditions characterized by $\dot{V}, \omega, h, P \geq 0$, as measurements for abnormal pump operating conditions are scarce and normal pump operating conditions are of primary interest. The model uses quadratic polynomials for the approximation of homologeous head h/ω^2 and homologeous power $P/(\rho\omega^3)$ as a function of homologeous discharge $\dot{V}/\omega$:

$$\frac{h}{\omega^2} = \tilde{c}_{h,0} + \tilde{c}_{h,1}\frac{\dot{V}}{\omega} + \tilde{c}_{h,2}\left(\frac{\dot{V}}{\omega}\right)^2, \quad (1)$$

$$\frac{P}{\rho\omega^3} = \frac{\tau\omega}{\rho\omega^3} = \tilde{c}_{P,0} + \tilde{c}_{P,1}\frac{\dot{V}}{\omega} + \tilde{c}_{P,2}\left(\frac{\dot{V}}{\omega}\right)^2, \quad (2)$$

where τ denotes the torque, and $\tilde{\boldsymbol{c}}_h = (\tilde{c}_{h,0}, \tilde{c}_{h,1}, \tilde{c}_{h,2})^\mathsf{T}$ and $\tilde{\boldsymbol{c}}_P = (\tilde{c}_{P,0}, \tilde{c}_{P,1}, \tilde{c}_{P,2})^\mathsf{T}$ are non-dimensionless coefficients. The head characteristic of a centrifugal pump is based on the linear Euler characteristic and extended by accounting for friction and shock losses, which can be well approximated by quadratic terms for centrifugal pumps, see e.g. (Kallesøe 2005, eq. (3.19)), (Sigloch 2013, fig. 9.5), (Gülich 2010, fig. 4.3), (Stepanoff 1957, fig. 9.8). Similarly, the torque characteristic is also found to follow a quadratic relationship (Kallesøe 2005, eq. (3.24)).

Equation 1 and Equation 2 can be rewritten in terms of normalized variables as:

$$h_\mathrm{n} = c_{h,0}\omega_\mathrm{n}^2 + c_{h,1}\omega_\mathrm{n}\dot{V}_\mathrm{n} + c_{h,2}\dot{V}_\mathrm{n}^2, \quad (3)$$

$$P_\mathrm{n} = \omega_\mathrm{n}\tau_\mathrm{n} = \omega_\mathrm{n}\rho_\mathrm{n}\left(c_{P,0}\omega_\mathrm{n}^2 + c_{P,1}\omega_\mathrm{n}\dot{V}_\mathrm{n} + c_{P,2}\dot{V}_\mathrm{n}^2\right), \quad (4)$$

where $h_\mathrm{n} = h/h_\mathrm{ref}$, $\dot{V}_\mathrm{n} = \dot{V}/\dot{V}_\mathrm{ref}$, $\omega_\mathrm{n} = \omega/\omega_\mathrm{ref}$, $P_\mathrm{n} = P/P_\mathrm{ref}$, $\tau_\mathrm{n} = \tau/\tau_\mathrm{ref}$, and $\rho_\mathrm{n} = \rho/\rho_\mathrm{ref}$ are the normalized head, discharge, speed, power, torque, and fluid density, respectively, h_ref, $\dot{V}_\mathrm{ref}$, ω_ref, $P_\mathrm{ref} = \tau_\mathrm{ref}\omega_\mathrm{ref}$, and ρ_ref are the corresponding reference values and $\boldsymbol{c}_h = (c_{h,0}, c_{h,1}, c_{h,2})^\mathsf{T}$ and $\boldsymbol{c}_P = (c_{P,0}, c_{P,1}, c_{P,2})^\mathsf{T}$ are dimensionless coefficients.

From a mathematical perspective, reference values can be chosen arbitrarily. In practice, however, they are chosen at the point of best efficiency, also referred to as the rated conditions (Chaudhry 2014, sec. 4.3), (Stepanoff 1957). This normalization facilitates the comparison of different pumps, as similar pumps will exhibit similar normalized characteristics. The effect of impeller diameter D on performance, described by head $h \sim D^2$, discharge $\dot{V} \sim D^3$, and power $P \sim D^5$, is implicitly accounted for through these reference quantities. Therefor pump scaling can be accomplished by adapting the reference values accordingly.

An additional advantage of Equation 3 and Equation 4 is the avoidance of division by zero at zero discharge $\dot{V} = 0$ and/or zero speed $\omega = 0$, which is essential for initializing simulations from rest. This contrasts with models within `Modelica.Fluid`, as noted in (Wetter 2013). Furthermore, using polynomials of degree higher than two would either violate the affinity laws or necessitate additional numerical handling to prevent division by zero.

It is also worth noting that, unlike in (Wetter 2013), Equation 3 is not constrained to be monotonically decreasing. Although the presence of a maximum can lead to dynamic instability to be avoided in practice, it is a physically observed phenomenon for centrifugal pumps. While steady-state solvers may fail to converge at this point, the TFS library does not assume steady-state conditions. Instead, it incorporates the fluid inertia by default and is capable of capturing transient behaviors such as surge limit cycles. Consequently, the numerical workarounds described in (Wetter 2013) become unnecessary. Nevertheless, Equation 3 and Equation 4 require modification to qualitatively account for reverse operation with discharge $\dot{V} < 0$, as discussed in section 3. In order to quantitatively cover all four quadrants of pump operation, it might be worthwhile to integrate the approach presented in (Chaudhry 2014, sec. 4.3) into the TFS in the future. Finally, pump efficiency is defined as $\eta = \rho g h \dot{V}/P$, where g is the standard gravitational acceleration.

DOI 10.3384/ecp218325

2.2 Approximation based on measurement data

The six coefficients of the quadratic head and power approximation polynomials $\boldsymbol{c}_h = (c_{h,0}, c_{h,1}, c_{h,2})^\intercal$ and $\boldsymbol{c}_P = (c_{P,0}, c_{P,1}, c_{P,2})^\intercal$ can each be determined by solving a quadratic polynomial regression, i.e. solving the linear equation systems $\boldsymbol{A}^\intercal\boldsymbol{A}\boldsymbol{c}_h = \boldsymbol{A}^\intercal\boldsymbol{b}_h$ and $\boldsymbol{A}^\intercal\boldsymbol{A}\boldsymbol{c}_P = \boldsymbol{A}^\intercal\boldsymbol{b}_P$ for the coefficients $\boldsymbol{c}_h$ and $\boldsymbol{c}_P$ respectively, where the matrix elemets $A_{ij} = (\dot{V}_i/(\dot{V}_{\mathrm{ref}}\omega_{\mathrm{n},i}))^{j-1}$ and the vector elements $b_{h,i} = h_i/(h_{\mathrm{ref}}\omega_{\mathrm{n},i}^2)$ and $b_{P,i} = P_i/(P_{\mathrm{ref}}\omega_{\mathrm{n},i}^3)$. Thereby h_i, $\dot{V}_i$, ω_i and P_i are measurements of head, discharge, speed and power respectively and $\omega_{\mathrm{n},i} = \omega_i/\omega_{\mathrm{ref}}$ is the normalized measured speed. If only measurements at reference speed ω_{ref} are used, the normalized speed $\omega_{\mathrm{n},i} = 1$. The reference quantities h_{ref}, $\dot{V}_{\mathrm{ref}}$ and P_{ref} can e.g. be defined at maximum measured efficiency $\eta_{\mathrm{ref}} = \max \rho g h_i \dot{V}_i / P_i$, which has advantages that are shown subsequently. In addition reference quantities improve the condition number of the matrix $\boldsymbol{A}$, since coefficients $\boldsymbol{c}_h$ and $\boldsymbol{c}_P$ are then dimensionless and approximately of the same magnitude.

Figure 2 shows measurements and approximation polynomials of a sample development pump from the automotive supplier HELLA GmbH & Co. KGaA. It shows head h, efficiency η and power P in dependency of discharge $\dot{V}$ and normalized head h/ω_{n}^2, efficiency η and normalized power P/ω_{n}^3 in dependency of normalized discharge $\dot{V}/\omega_{\mathrm{n}}$. The reference speed was arbitrarily chosen as $\omega_{\mathrm{ref}} = 5440\,\mathrm{rpm}$ and the reference density $\rho_{\mathrm{ref}} = 1000\,\mathrm{kg/m^3}$. Different colors refer to different speeds ω and measurement data are highlighted with markers. Approximation 1 (solid) is based on measurements at reference speed $\omega_{\mathrm{ref}} = 5440\,\mathrm{rpm}$ only. In contrast approximation 2 (dashed) is based on measurements at all eight speeds $\omega = 2040\,\mathrm{rpm}$ to $6800\,\mathrm{rpm}$. Figure 2 shows that a transformation based on affinity laws projects the head, efficiency and power maps well onto single curves, i.e. the homologeous quantities can be well expressed as a function of homologeous discharge $\dot{V}/\omega_{\mathrm{n}}$. This is especially true for the head h. In contrast applying affinity laws for power P overestimates the efficiency η for low speeds, but the results might still be accurate enough if off design power at low speed is of minor importance. Also note that the available torque data at those low speeds had only one significant digit.

If reference power P_{ref} is defined as $P_{\mathrm{ref}} = \rho_{\mathrm{ref}} g h_{\mathrm{ref}} \dot{V}_{\mathrm{ref}}/\eta_{\mathrm{ref}}$ one can derive that the efficiency:

$$\eta = \eta_{\mathrm{ref}} \frac{x + c_h x^2 - (1 + c_h) x^3}{c_{P,1} + c_{P,2} x + c_{P,3} x^2}, \tag{5}$$

where $x = \dot{V}_{\mathrm{n}}/\omega_{\mathrm{n}}$ is the homologeous discharge. Hence applying affinity laws yields efficiency $\eta \sim \dot{V}/\omega$, as already shown in Figure 2. Consequently according to affinity laws efficiency $\eta \sim \dot{V}/\sqrt{h}$, since head $h \sim \omega^2$. Therefor curves of constant efficiency η are parabolas $h = c(\eta)\dot{V}^2$, where $c(\eta)$ is a parameter, see e.g. (Sigloch 2013, sec. 9.2).

Figure 3 shows the approximated map of a sample development pump from the automotive supplier HELLA GmbH & Co. KGaA based on measurements at reference speed $\omega_{\mathrm{ref}} = 5440\,\mathrm{rpm}$ only (equivalent to approximation 1 in Figure 2) and extended using affinity laws. Solid lines thereby refer to the same curves of constant speed ω as displayed in Figure 2. The reference speed line $\omega = \omega_{\mathrm{ref}}$ is displayed as thick solid. Dashed lines refer to parabolas of constant efficiency η and numbers 0.2, 0.5, 0.8, 0.9, 0.95 and 1 refer to the ratio of efficiency to peak efficiency η/η_{ref}. The peak efficiency curve $\eta = \eta_{\mathrm{ref}}$ is displayed as thick dashed.

Even if the dashed parabolas of constant efficiency in Figure 3 represent the principal pump behavior, it is well known that the efficiency decreases for off design speeds $\omega > \omega_{\mathrm{ref}}$ and $\omega < \omega_{\mathrm{ref}}$, yielding the well known pump map shape, see e.g. (Sigloch 2013, fig. 9-14). This is not yet considered by the model, but by means of a simple modification the model could in the future be improved by a efficiency reduction coefficient $c(\omega) \leq 1$ reducing the peak efficiency of individual speed curves $\eta_{\mathrm{ref}}(\omega) = c(\omega)\eta_{\mathrm{ref}}(\omega_{\mathrm{ref}})$.

Figure 2 furthermore shows, that for (radial flow) centrifugal pumps quadratic polynomials are suitable for the approximation. However note, that quadratic polynomials may not be suitable to approximate pumps with higher specific speed, e.g. mixed flow or axial flow pumps, since their characteristics may differ considerably, see e.g. (Sigloch 2013, fig. 9-16). Specific speed is thereby defined as (Chaudhry 2014):

$$\omega_{\mathrm{specific}} = \omega \sqrt{\frac{\dot{V}}{\sqrt{gh}^3}}. \tag{6}$$

Note that the sample development pump from the automotive supplier HELLA GmbH & Co. KGaA has a specific speed of 0.406.

Figure 4 shows mean relative errors of the approximations as shown in Figure 2 for series of measurements at constant speed ω. Colors correspond to head h (blue), power P (red) and efficiency η (black). As in Figure 2 approximation 1 (solid) is also in Figure 4 based on measurements at reference speed $\omega_{\mathrm{ref}} = 5440\,\mathrm{rpm}$ only and approximation 2 (dashed) is based on measurements at all eight speeds $\omega = 2040\,\mathrm{rpm}$ to $6800\,\mathrm{rpm}$. Figure 4 shows that the mean relative error regarding head h is for all speeds about one order of

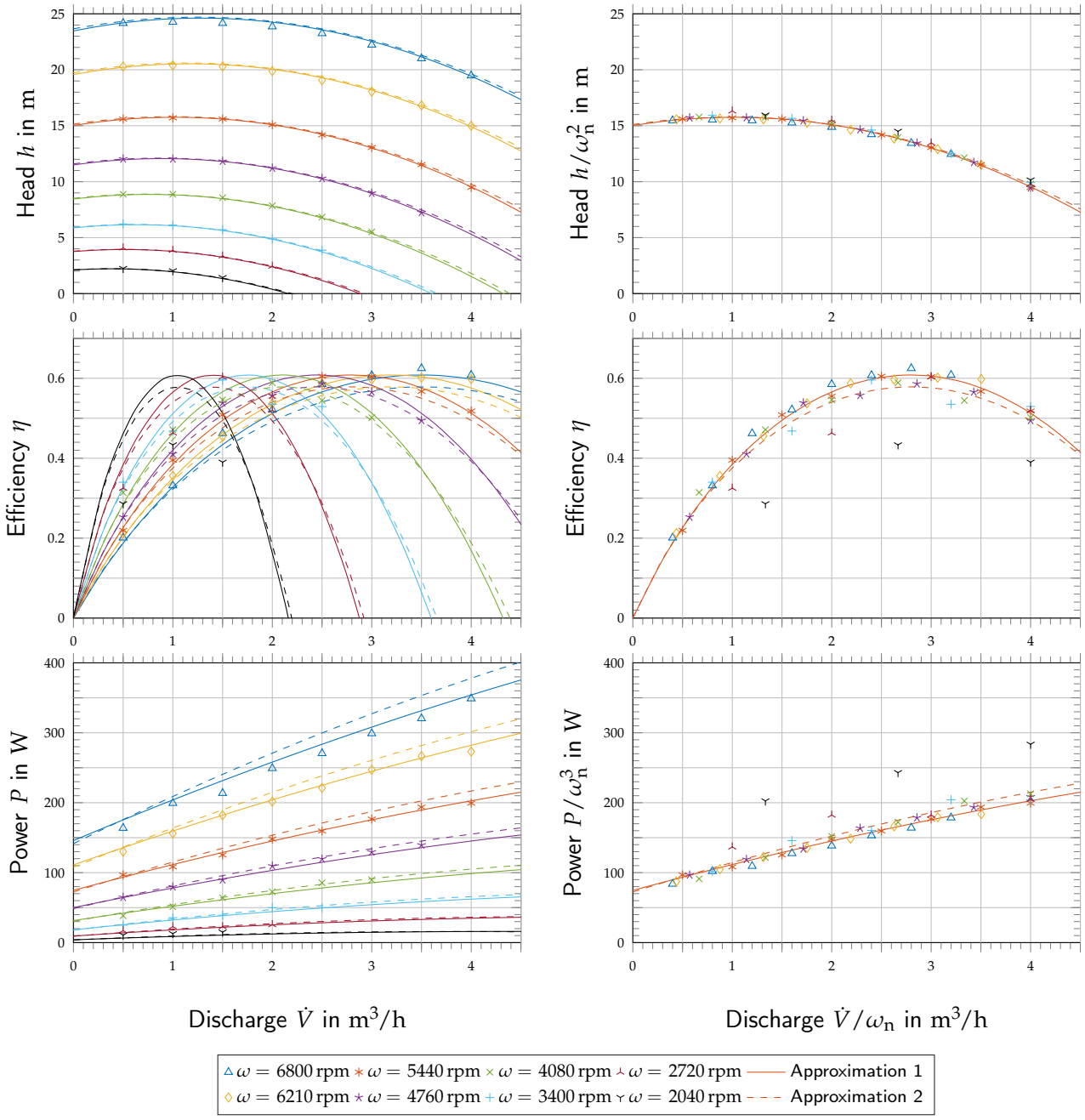

Figure 2. Measurements and approximation polynomials of a sample development pump from the automotive supplier HELLA GmbH & Co. KGaA.

magnitude smaller than the mean relative error regarding power P and efficiency η. The strongest outlier regarding head h is only 6.0 % and 4.0 % off for approximation 1 and 2 respectively, which is remarkable considering that the available head data at low speeds had only 2 significant digits. Including measurements at all eight speeds changes the mean error on average only slightly from $\mathrm{err}_{h,\mathrm{ap1}} = 1.5\,\%$ to $\mathrm{err}_{h,\mathrm{ap2}} = 1.3\,\%$ regarding head h, from $\mathrm{err}_{P,\mathrm{ap1}} = 8.2\,\%$ to $\mathrm{err}_{P,\mathrm{ap2}} = 8.7\,\%$ regarding power P, and from $\mathrm{err}_{\eta,\mathrm{ap1}} = 9.4\,\%$ to $\mathrm{err}_{\eta,\mathrm{ap2}} = 7.7\,\%$ regarding efficiency η, where the subscripts $(\bullet)_{\mathrm{ap1}}$ and $(\bullet)_{\mathrm{ap2}}$ refer to the first and second approximation respectively. This demonstrates that the approximation can not really be improved by including measurements at different speeds. However both approximations yield significant errors concerning power and efficiency of up to 40 % at low speeds, which highlights the need to extend the model as previously mentioned, if off design power and efficiency at low speeds matter.

2.3 Comparison of centrifugal pumps

A convenient way to obtain the six head and power coefficients $\boldsymbol{c}_h$ and $\boldsymbol{c}_P$ can be achieved by defining:

DOI 10.3384/ecp218325

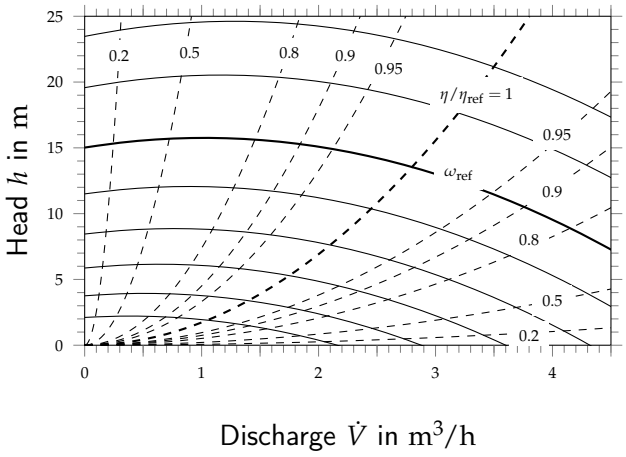

Figure 3. Map of a sample development pump from the automotive supplier HELLA GmbH & Co. KGaA.

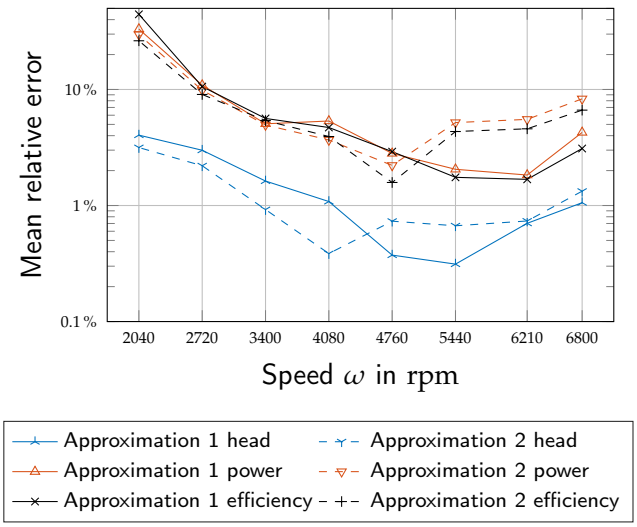

Figure 4. Mean relative errors of the approximations as shown in Figure 2 for series of measurements at constant speed ω.

1. the peak efficiency η_{ref}
2. the head at peak efficiency h_{ref}
3. the discharge at peak efficiency $\dot{V}_{\text{ref}}$
4. the normalized head at zero discharge $h_{0,\text{n}}$
5. the normalized discharge at zero head $\dot{V}_{0,\text{n}}$
6. the normalized power at zero discharge $P_{0,\text{n}}$

Items 2 to 5 provide three equations for the head coefficients $\boldsymbol{c}_h$, which yield:

$$c_{h,0} = h_{0,\text{n}}\,, \tag{7}$$

$$c_{h,1} = \frac{\dot{V}_{0,\text{n}}}{\dot{V}_{0,\text{n}} - 1} - h_{0,\text{n}} \frac{\dot{V}_{0,\text{n}} + 1}{\dot{V}_{0,\text{n}}}\,, \tag{8}$$

$$c_{h,2} = \frac{h_{0,\text{n}}}{\dot{V}_{0,\text{n}}} - \frac{1}{\dot{V}_{0,\text{n}} - 1}\,, \tag{9}$$

Table 1. Parameters of approximation 1 (ap1) and approximation 2 (ap2) of the sample development pump from the automotive supplier HELLA GmbH & Co. KGaA. as shown in Figure 2. The reference speed $\omega_{\text{ref}} = 5440\,\text{rpm}$ and the reference density $\rho_{\text{ref}} = 1000\,\text{kg/m}^3$.

	h_{ref} in m	$\dot{V}_{\text{ref}}$ in m³/h	η_{ref} in %	$h_{0,\text{n}}$	$\dot{V}_{0,\text{n}}$	$P_{0,\text{n}}$
ap1	13.5	2.80	60.8	1.11	2.06	0.440
ap2	13.6	2.80	57.9	1.11	2.09	0.403

Table 2. Mean, standard deviation, minimum and maximum values of normalized head at zero discharge $h_{\text{n},0}$, normalized discharge at zero head $\dot{V}_{\text{n},0}$ and normalized power at zero flow $P_{\text{n},0}$ for 18 WILO pumps available in the Modelica Buildings Library (Wetter et al. 2014) .

	mean	std	min	max
$h_{0,\text{n}}$	1.273	±0.128	1.101	1.516
$\dot{V}_{0,\text{n}}$	1.946	±0.087	1.784	2.090
$P_{0,\text{n}}$	0.499	±0.099	0.372	0.677

and items 1 and 6 provide three more equations for the power coefficients $\boldsymbol{c}_P$, which yield:

$$c_{P,0} = P_{0,\text{n}}\,, \tag{10}$$

$$c_{P,1} = -2P_{0,\text{n}} + c_{h,0} - c_{h,2}\,, \tag{11}$$

$$c_{P,2} = P_{0,\text{n}} + c_{h,1} + 2c_{h,2}\,. \tag{12}$$

Table 1 summarizes the parameters of approximation 1 (ap1) and approximation 2 (ap2) of the sample development pump from the automotive supplier HELLA GmbH & Co. KGaA. as shown in Figure 2. Those six coefficients (plus reference speed $\omega_{\text{ref}} = 5440\,\text{rpm}$ and the reference density $\rho_{\text{ref}} = 1000\,\text{kg/m}^3$) are sufficient to fully describe the pump characteristic.

The benefit of this approach is, that head at design point h_{ref} and discharge at design point $\dot{V}_{\text{ref}}$ may vary for different pumps according to their requirements. For example the design points of the 18 WILO pumps available in the Modelica Buildings Library differ significantly: their peak head h_{ref} ranges from 1.4 m up to 22 m, their peak discharge ranges $\dot{V}_{\text{ref}}$ from 2.9 m³/h up to 73 m³/h, their peak power P_{ref} ranges from 27 W up to 4.2 kW and their peak efficiency η_{ref} ranges from 24 % up to 77 %. However the three coefficients: 1) normalized head at zero discharge $h_{\text{n},0}$, normalized discharge at zero head $\dot{V}_{\text{n},0}$ and normalized power at zero flow $P_{\text{n},0}$ differ much less as listed in Table 2. Hence normalized pump characteristics differ only to a medium degree as shown in Figure 5 for 18 WILO pumps available in the Modelica Buildings Library (Wetter et al. 2014). Colors in Figure 5 refer to different pumps and the pump characteristics based on mean parameters as

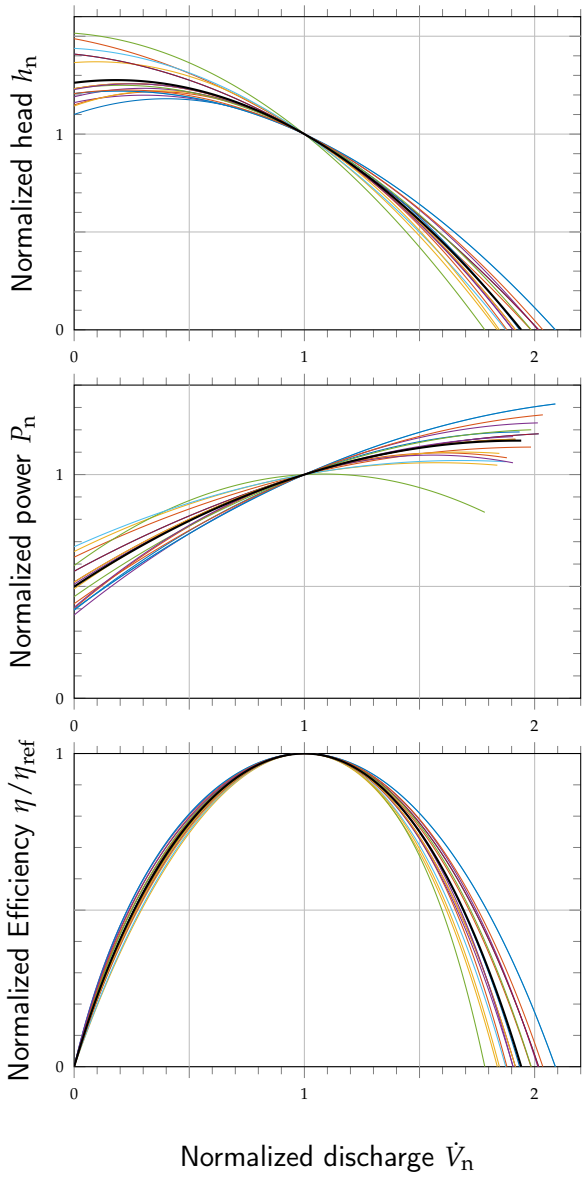

Figure 5. Comparison of 18 WILO pumps available in the Modelica Building Library (Wetter et al. 2014).

listed in Table 2 are marked thick black. The similarity is also based on the fact that the specific speed only varies from 0.42 to 1.21.

Note that (Sigloch 2013, sec. 9.2) also mentions a range of normalized power at zero flow of $P_{0,n} = 0.4$ to 0.6. The peak efficiency η_{ref} is also rather easy to predict where smaller and/or cheaper pumps usually reach lower peak efficiencies and larger, more efficient pumps can reach up to 90 % peak efficiency.

3 Example: Instationary behavior

To extend the pump map to negative discharge $\dot{V} < 0$, we adopt the head characteristic of Equation 3 by replacing the square term $\dot{V}_n^2$ by $\dot{V}_n|\dot{V}_n|$:

$$h_n = c_{h,0}\omega_n^2 + c_{h,1}\omega_n\dot{V}_n + c_{h,2}\dot{V}_n|\dot{V}_n|. \qquad (13)$$

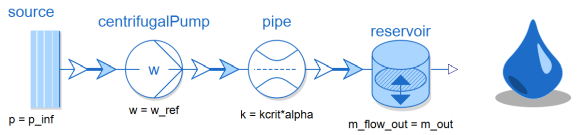

Figure 6. Exemplary system to investigate instationary pump behavior.

Note that this modification is a rather simple qualitative extension for negative discharge $\dot{V} < 0$ that is still able to predict the principle physical behavior as the quadratic term originates from friction that is $\sim \dot{V}|\dot{V}|$, see (Sigloch 2013, sec. 9.2). In order to quantitatively cover all four quadrants of pump operation, it might be worthwhile to integrate the approach presented in (Chaudhry 2014, sec. 4.3) into the TFS in the future.

Figure 6 shows an exemplary system to investigate instationary pump behavior. An open reservoir with a constant discharge `m_flow_out` $= \rho\dot{V}_{out}$ is fed through a flow resistance by a centrifugal pump at constant speed `w_ref` $= \omega_{ref}$. Depending on the constant discharge $\dot{V}_{out}$ and on the flow resistance the system may yield a limit cycle known as surge, such that the system does not reach a steady-state (Sigloch 2013, sec. 9.2). In this case the system can only be simulated when considering dynamic effects.

In the following we use head at zero discharge as new reference head $\hat{h}_{ref}$ and discharge at zero head as new reference discharge $\hat{V}_{ref}$:

$$\hat{h}_{ref} = h_{ref}c_{h,0}, \qquad (14)$$

$$\hat{V}_{ref} = \frac{\dot{V}_{ref}}{2c_{h,2}}\left(-c_{h,1} - \sqrt{c_{h,1}^2 - 4c_{h,0}c_{h,2}}\right), \qquad (15)$$

which simplifies Equation 13:

$$\hat{h}_n = \omega_n^2 + \hat{c}\omega_n\hat{\dot{V}}_n - (1+\hat{c})\hat{\dot{V}}_n|\hat{\dot{V}}_n|, \qquad (16)$$

where $\hat{h}_n = h/\hat{h}_{ref}$ and $\hat{\dot{V}}_n = \dot{V}/\hat{\dot{V}}_{ref}$ are normalized head and discharge and $\hat{c}$ is a coefficient:

$$\hat{c} = c_{h,1}\frac{h_{ref}\hat{\dot{V}}_{ref}}{\hat{h}_{ref}\dot{V}_{ref}}. \qquad (17)$$

The limit cycle can only occur when the discharge $\dot{V}_{out}$ is less than the critical discharge at maximum head $\dot{V}_{out} \leq \dot{V}_{crit}$. The corresponding critical normalized discharge can be derived based on the condition $\mathrm{d}\hat{h}_n/\mathrm{d}\hat{\dot{V}}_n = 0$ at reference speed $\omega_n = 1$ as:

$$\hat{\dot{V}}_{n,crit} = \frac{\hat{c}}{2(1+\hat{c})}. \qquad (18)$$

We consider a constant reservoir discharge $\dot{V}_{out} = 1/2\dot{V}_{crit}$ such that surge may occur depending on the system characteristics.

DOI 10.3384/ecp218325

Surge occurs, if the pump- and system characteristics do not intersect anymore. In the limiting case that means that pump- and system characteristics are tangential for the constant reservoir discharge $\dot{V}_{\text{out}}$:

$$\left.\frac{\mathrm{d}\hat{h}_{\text{p,n}}}{\mathrm{d}\hat{V}_{\text{n}}}\right|_{\hat{V}_{\text{out,n}}} = \left.\frac{\mathrm{d}\hat{h}_{\text{sys,n}}}{\mathrm{d}\hat{V}_{\text{n}}}\right|_{\hat{V}_{\text{out,n}}}, \tag{19}$$

where $\hat{h}_{\text{p,n}} = h_{\text{p}}/\hat{h}_{\text{ref}}$, $\hat{h}_{\text{sys,n}} = h_{\text{sys}}/\hat{h}_{\text{ref}}$ and $\hat{V}_{\text{out,n}} = \dot{V}_{\text{out}}/\hat{V}_{\text{ref}}$ are the normalized pump head, system head, and reservoir discharge.

To be able to derive analytical results later on, we assume a constant friction factor k for the system characteristics. Furthermore the normalized friction factor $\hat{k}$ is introduced:

$$\Delta p_{\text{sys}} = k\dot{m}\,|\dot{m}|\,, \tag{20}$$

$$\implies \hat{h}_{\text{sys,n}} = \hat{k}\hat{V}_{\text{n}}\left|\hat{V}_{\text{n}}\right|, \quad \hat{k} = k\frac{\rho\hat{V}_{\text{ref}}^2}{g\hat{h}_{\text{ref}}}. \tag{21}$$

Then Equation 19 yields the critical normalized friction factor $\hat{k}_{\text{crit}}$:

$$\hat{k}_{\text{crit}} = \frac{\hat{c}}{2|\hat{V}_{\text{out,n}}|} - (1+\hat{c}), \tag{22}$$

such that a normalized friction factor $\hat{k} \leq \hat{k}_{\text{crit}}$ yields surge.

Figure 7 shows simulation results of the exemplary system (Figure 6) for five different friction factors $k = \alpha k_{\text{crit}}$ with coefficient $\alpha = 0$, 0.5, 0.98, 1.02 and 2 (different colors). The ambient pressure `p_inf` $= p_\infty = 1\,\text{bar}$, the cross sectional area of the reservoir $A = 100\,\text{cm}^2$, the initial height of the reservoir $h_{\text{R},0} = 13\,\text{m}$, the initial pump discharge $\dot{V}(0) = 0\,\text{m}^3/\text{s}$, the density and reference density are $\rho = \rho_{\text{ref}} = 1000\,\text{kg}/\text{m}^3$ and the overall inertance $L = (4 \times 0.01)/\text{m}$. The constant reservoir discharge $\dot{V}_{\text{out}} = 0.5\dot{V}_{\text{crit}} = 0.512\,\text{m}^3/\text{h}$ yields a critical friction factor `kcrit` $= k_{\text{crit}} = 8.92 \times 10^4\,\text{Pa}\,\text{s}^2/\text{kg}^2$. The example is a second order system of nonlinear differential equations:

$$L\rho\frac{\mathrm{d}\dot{V}}{\mathrm{d}t} = \Delta p_{\text{p}} - (\Delta p_{\text{sys}} + \rho g h_{\text{R}}), \tag{23}$$

$$A\frac{\mathrm{d}h_{\text{R}}}{\mathrm{d}t} = \dot{V} - \dot{V}_{\text{out}}. \tag{24}$$

Note that the implicit part is linear (it is even diagonal and regular for $L, A \neq 0$), so it is a trivial task to solve the system for its states $\boldsymbol{x} = (\dot{V}, h_{\text{R}})^{\intercal}$, which is generally the case for the TFS.

Figure 7 shows that discharge $\dot{V}$ increases quickly from rest and reaches a quasi-static equilibrium shortly after initialization, since the flow rate dynamics limited by the inertance L are a lot faster than the reservoir dynamics and hence often the influence of the flow rate dynamics can be neglected and the system is quasi-static with respect to the flow rate dynamics.

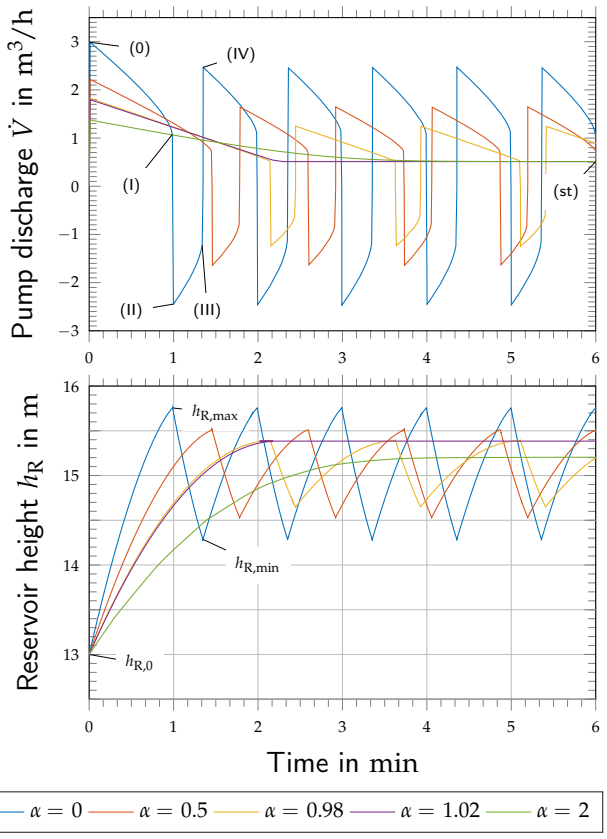

Figure 7. Instationary pump simulation for different pipe characteristics.

The initial quasi-static discharge $\dot{V}_{0+}$ depends on the system characteristics and hence on the coefficient α. The higher the coefficient α, i.e. the more friction, the lower the initial quasi-static discharge $\dot{V}_{0+}$. Afterwards the reservoir height h_{R} increases (time $t \leq (1 \text{ to } 2)\,\text{min}$) and the discharge $\dot{V}$ decreases. For coefficients $\alpha = 1.02$ and 2 the pump discharge $\dot{V}$ decreases until it balances the reservoir discharge $\dot{V}_{\text{out}}$ and the system reaches steady-state (st). The larger the coefficient α, i.e. the more friction, the lower is the steady-state reservoir height $h_{\text{R,st}}$.

In contrast for coefficients $\alpha = 0$, 0.5 and 0.98 the system yields a limit cycle, with critical points (I), (II), (III) and (IV). Note that the critical discharges $\dot{V}_{\text{I}}$ to $\dot{V}_{\text{IV}}$, the critical minimum and maximum reservoir heights $h_{\text{R,min}}$ and $h_{\text{R,max}}$, the periods of the positive and negative limit cycle T_+ and T_- and the overall period $T = T_+ + T_-$ depend on the coefficient α.

Figure 8 illustrates the quasi-static system behavior, defined by the intersection of the system characteristics (dotted) and the pump characteristics (solid). The three subplots and their respec-

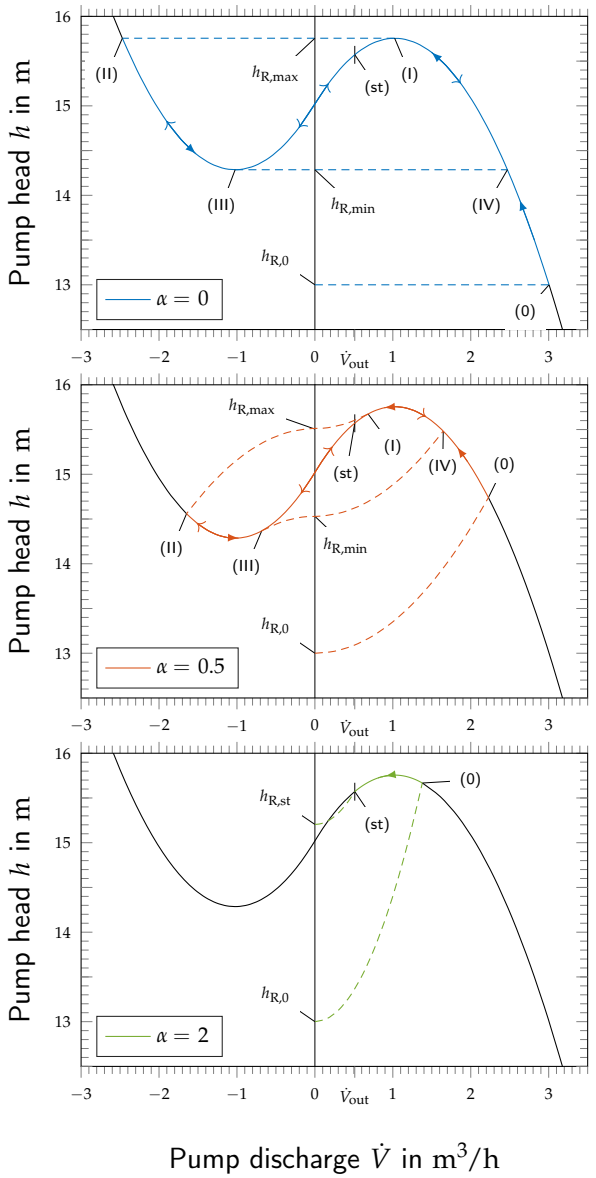

Figure 8. System behaviour for different pipe characteristics.

tive colors correspond to the three values of the coefficient $\alpha = 0$, 0.5 and 2. The y-axis intercept of the system characteristics represents the reservoir height h_R, and the curvature is proportional to the coefficient α. In contrast, all three subplots share the same pump characteristic since the pump speed ω is identical.

Initially, it can be observed that different values of α lead to different quasi-static initial discharges (0), resulting in different initial net inflows to the reservoir $\dot{V}_{0+} - \dot{V}_{out}$. Consequently, the reservoir height h_R increases more rapidly for $\alpha = 0$ compared to $\alpha = 2$. As the reservoir height h_R increases, the system characteristics shift vertically. The new intersection between the shifted system characteristics and the pump characteristics results in a decreasing pump discharge $\dot{V}$, thereby slowing the increase of the reservoir height h_R. This quasi-static evolution is indicated by filled arrows (⟶).

For $\alpha = 2$, the system eventually reaches the steady-state point (st), where the net inflow $\dot{V} - \dot{V}_{out}$ becomes zero, and the reservoir height h_R remains constant. This point is stable because any small deviation would still lead to an intersection between system and pump characteristics, generating a restoring effect that drives the system back to steady state.

In contrast, for $\alpha = 0$ and 0.5, the system reaches the critical point (I) before achieving steady state (st). At this point, the net reservoir inflow $\dot{V} - \dot{V}_{out}$ remains positive, and the reservoir height h_R continues to rise. However, beyond the critical point (I), no quasi-static intersection exists. The reservoir pressure decelerates the fluid, reducing the pump discharge $\dot{V}$, which in turn further decelerates and eventually reverses the flow. A new quasi-static equilibrium is reached only at the reversed pump discharge (II). During the rapid transition from (I) to (II), the pump (solid) and system (dashed) characteristics remain valid, and the pressure difference between them causes a sharp deceleration of the fluid. Meanwhile, the reservoir height remains approximately constant $h_R = h_{R,max}$. This fast transition is marked with arrows (⟶).

At point (II), the net inflow $\dot{V} - \dot{V}_{out}$ becomes negative, causing the reservoir height h_R to decrease. The intersection between the shifted system characteristics and the pump characteristics now evolves quasi-statically again (⟶). However, before reaching steady state (st), the system encounters the next critical point (III). At this point, the reservoir height h_R becomes too low to sustain reversed flow through the pump. The fluid is then accelerated by the pump, increasing the discharge $\dot{V}$, which further accelerates the fluid until a new quasi-static intersection is reached at point (IV). During the rapid transition from (III) to (IV), the pump (solid) and system (dashed) characteristics are again satisfied. The resulting pressure difference drives the flow reversal, while the reservoir height remains approximately constant $h_R = h_{R,min}$. This fast transition is indicated by arrows (⟶). The limit cycle then repeats, preventing the system from reaching the steady-state point (st).

3.1 Analytic verification

The behavior is well known, see e.g. (Sigloch 2013, sec. 9.2). To confirm the previous simulation results, analytic results are derived in the following.

First note that the critical discharges $\dot{V}_I$ to $\dot{V}_{IV}$ and the maximum and minimum reservoir heights $h_{R,max}$ and $h_{R,min}$ can be determined analytically by evaluating Equation 19 for given

normalized friction factor $\hat{k}$, which yields:

$$\hat{V}_{\mathrm{I,n}} = \frac{\hat{c}}{2(1+\hat{c}+\hat{k})}, \tag{25}$$

$$\hat{h}_{\mathrm{R,max,n}} = 1 + \hat{c}\hat{V}_{\mathrm{I,n}} - (1+\hat{c}+\hat{k})\hat{V}_{\mathrm{I,n}}^2, \tag{26}$$

$$\hat{V}_{\mathrm{II,n}} = \frac{\hat{c} + \sqrt{\hat{c}^2 - 4(1+\hat{c}+\hat{k})\left(1-\hat{h}_{\mathrm{R,max,n}}\right)}}{-2(1+\hat{c}+\hat{k})}, \tag{27}$$

$$\hat{V}_{\mathrm{III,n}} = -\hat{V}_{\mathrm{I,n}}, \tag{28}$$

$$\hat{V}_{\mathrm{IV,n}} = -\hat{V}_{\mathrm{II,n}}, \tag{29}$$

$$\hat{h}_{\mathrm{R,min,n}} = 1 - (\hat{h}_{\mathrm{R,max,n}} - 1). \tag{30}$$

Solving the second order system of nonlinear differential equations (Equation 23 and Equation 24) analytically is not trivial, but neglecting the flow rate dynamics, i.e. for zero interance $L = 0$, Equation 23 becomes analytic. Then one combine Equation 23 and Equation 24 and derive the first order nonlinear differential equation for the normalized reservoir height $\hat{h}_{\mathrm{R,n}}$:

$$\frac{\mathrm{d}\hat{h}_{\mathrm{R,n}}}{\mathrm{d}\tau} = -\hat{V}_{\mathrm{out,n}} \pm \hat{V}_{\mathrm{I,n}}\left(1 + \sqrt{1 \pm \gamma(1-\hat{h}_{\mathrm{R,n}})}\right), \tag{31}$$

where $\tau = t/t_{\mathrm{ref}}$ is the normalized time, $t_{\mathrm{ref}} = A\hat{h}_{\mathrm{ref}}/\hat{V}_{\mathrm{ref}}$ is the reference time, $\gamma = 4(1+\hat{c}+\hat{k})/\hat{c}^2$ is a coefficient and $(\pm)$ refers to the positive branch $\dot{V} > 0$ and negative branch $\dot{V} < 0$ of the limit cycle respectively. The first order differential Equation 31 can be solved analytically for each branch of the limit cycle, and one can obtain an implicit solution of the normalized reservoir height $\hat{h}_{\mathrm{R,n}}$ depending on the normalized time τ:

$$\tau = f_{\pm}(\hat{h}_{\mathrm{R,n}}) - f_{\pm}(\hat{h}_{\mathrm{R,0,n}}), \tag{32}$$

$$f_{\pm} = -\frac{2}{\hat{V}_{\mathrm{I,n}}^2\gamma}\Big(\hat{V}_{\mathrm{I,n}}g_{\pm} + \\ + (\pm\hat{V}_{\mathrm{out,n}} - \hat{V}_{\mathrm{I,n}})\ln\left|\mp\hat{V}_{\mathrm{out,n}} + \hat{V}_{\mathrm{I,n}}(1+g_{\pm})\right|\Big), \tag{33}$$

$$g_{\pm} = \sqrt{1 \pm \gamma(1-\hat{h}_{\mathrm{R,n}})}, \tag{34}$$

where f and g are auxiliary variables and $\hat{h}_{\mathrm{R,0,n}}$ is the initial normalized reservoir height. This also enables the calculation of the periods corresponding to the positive and negative branches of the limit cycle $T_{\pm}$:

$$T_+/t_{\mathrm{ref}} = f_+(\hat{h}_{\mathrm{R,max,n}}) - f_+(\hat{h}_{\mathrm{R,min,n}}), \tag{35}$$

$$T_-/t_{\mathrm{ref}} = f_-(\hat{h}_{\mathrm{R,min,n}}) - f_+(\hat{h}_{\mathrm{R,max,n}}), \tag{36}$$

and the overall period of the limit cycle $T = T_+ + T_-$, where $g_+(\hat{h}_{\mathrm{R,max,n}}) = g_-(\hat{h}_{\mathrm{R,min,n}}) = \sqrt{2}$ and $g_+(\hat{h}_{\mathrm{R,min,n}}) = g_-(\hat{h}_{\mathrm{R,max,n}}) = 0$.

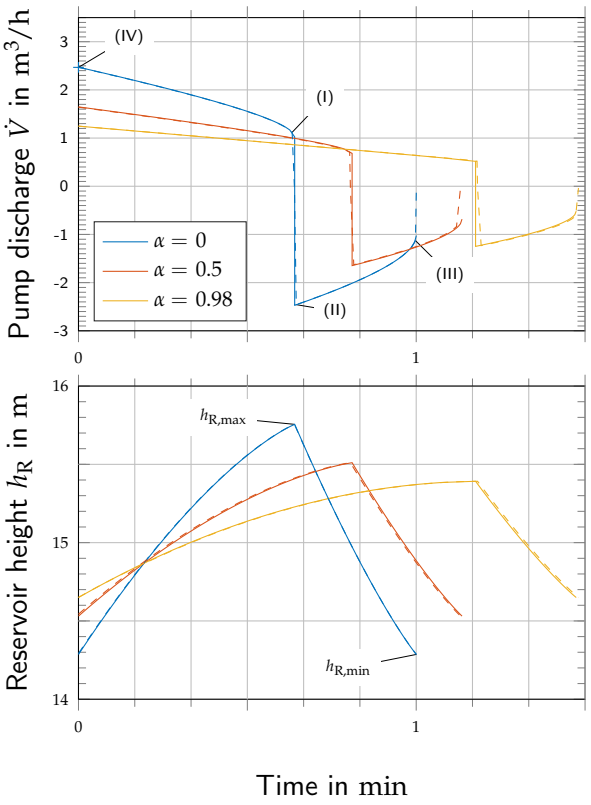

Figure 9. Comparison of analytical and dynamic simulation results for one limit cycle.

Figure 9 compares the analytic solution based on eqs. (32) to (34) (solid lines) with the numerical simulation results (dashed lines) of the first limit cycle as shown in Figure 7 that starts for $\alpha = 0$ at about 1 min 20 s, for $\alpha = 0.5$ at about 1 min 50 s and for $\alpha = 0.98$ at about 2 min 30 s. Colors refer to coefficients $\alpha = 0$, 0.5 and 0.98. Both results agree very well, i.e. Figure 9 verifies the analytic solution and the simulation model.

Figure 9 demonstrates, that the effect of the fluid inertia L is small, however considering its effect is crucial to solve the system. It is well known that nonlinear equation solvers may fail at the limit points (I) and (III), since a slight change in reservoir height $\dot{h}_{\mathrm{R}}$ causes a large change in discharge $\dot{V}$ if Equation 23 is solved algebraically ($L = 0$). There is no certainty that the solver of the nonlinear algebraic equation will converge at this step change in discharge. This is especially true for larger algebraic systems of nonlinear equations. When considering the effect of the fluid inertia the nonlinear algebraic equation turns into the differential equation. The implicit part of the system of differential equations is linear and it is a trivial task to solve for its states. From a physical point of view the dynamic equilibrium always exists and the implicit time integration method, which also has to solve a nonlinear equation system at every time step, is guided into the correct direction in

which the system will evolve. To be able to use an explicit time integration scheme the inertance L and the time step size have to match. In the future it might be promising to increase the inertance L up to a certain limit to enable real time simulation.

The example showed, that the simulation of limit cycles are possible with the TFS by default, since it takes the fluid inertia into account and avoids the common oversimplification of requiring quasi-static behavior. This actually simplifies the component models, since numerical modifications, as presented in (Wetter 2013), are no longer necessary. Note that while analytic calculations may help to verify simulation models for simple examples, modifications are very likely to cause analytic calculations to be neither possible nor feasible anymore. In these cases numerical simulation can still provide the opportunity to gain insight into system dynamics, if the simulation models proofed to be based on the correct physics.

4 Conclusion and Outlook

The proposed model for a centrifugal pump has proven to be a numerically robust model. The possibility to work with real pump behavior allows for instationary simulations. This is especially important when fault scenarios must be simulated. This also allows for a robust initialization of the models, as the model behavior follows the behavior from the real world. Fitting the pump data is simple, as no special care has to be taken to avoid instationary solutions, as the model can handle these well. An example of an instationary pump model has been validated against the theoretical solutions with an extremely well correlation. Furthermore, the models have been validated against data from measurements. The models have been validated for pump head, power and efficiency over a wide range of pump speeds: The pump head fit at all speeds stays very good (lower than 1 % relative error for speeds around ω_{ref}, lower than 3 % relative error at $\omega < \omega_{\text{ref}}/2$). The pump power fits the reference data well around ω_{ref} with errors of approximately 2 %. Even at $\omega = \omega_{\text{ref}}/2$ the error is smaller than 10 %. However at speeds below $\omega < \omega_{\text{ref}}/2$ the error quickly grows to around 40 %. A similar behavior can be seen for the pump efficiency: at $\omega_{\text{ref}}/2 < \omega < 1.25\omega_{\text{ref}}$ the relative error stays below 5.5 %, quickly growing to 45 % below half the reference speed. Hence it might be worth considering a decreasing peak efficiency at off design speeds as an extensions to similarity laws to obtain the well known pump characteristics. To further improve the model and quantitatively cover all four quadrants of pump operations, the approach presented in (Chaudhry 2014, sec. 4.3) is planned to be integrated into the TFS in the future.

Acknowledgements

This work was carried out as part of the European project **TheMa4HERA**. The project is supported by the Clean Aviation Joint Undertaking and its members. Funded by the European Union under Grant Agreement No. 101102008.

References

Casella, Francesco et al. (2006). "The Modelica Fluid and Media library for modeling of incompressible and compressible thermo-fluid pipe networks". In: *Proceedings of the 5th international modelica conference*, pp. 631–640.

Chaudhry, M. Hanif (2014). *Applied Hydraulic Transients*. 3rd ed. Springer New York. DOI: https://doi.org/10.1007/978-1-4614-8538-4.

Fu, Hongxiang, David Blum, and Michael Wetter (2023). "Fan and Pump Efficiency in Modelica based on the Euler Number". In.

Gülich, Johann Friedrich (2010). *Kreiselpumpen: Handbuch für Entwicklung, Anlagenplanung und Betrieb*. 3rd ed. Springer. DOI: 10.1007/978-3-642-05479-2.

Kallesøe, Carsten (2005). "Fault detection and isolation in centrifugal pumps". PhD thesis. Denmark: Aalborg University. URL: https://vbn.aau.dk/en/publications/fault-detection-and-isolation-in-centrifugal-pumps.

Karassik, Igor J. et al., eds. (2007). *Pump Handbook*. 4th ed. McGraw-Hill. ISBN: 978-0071460446.

Richter, Christoph C (2008). "Proposal of new object-oriented equation-based model libraries for thermodynamic systems". PhD thesis. Braunschweig, Techn. Univ.

Sigloch, Herbert (2013). *Strömungsmaschinen: Grundlagen und Anwendungen*. 8th ed. Carl Hanser Verlag GmbH Co KG. ISBN: 978-3-446-47677-6.

Stepanoff, Alexey Joakim (1957). *Centrifugal and Axial Flow Pumps: Theory, Design, and Application*. 2nd ed. John Wiley & Sons.

Trefethen, Lloyd N. (2019). "Chapter 13. Equispaced Points, Runge Phenomenon". In: *Approximation Theory and Approximation Practice, Extended Edition*. SIAM. Chap. 13, pp. 95–102. DOI: 10.1137/1.9781611975949.ch13.

Wetter, Michael (2013). "Fan and pump model that has a unique solution for any pressure boundary condition and control signal". In: *Building Simulation 2013*. Vol. 13. IBPSA, pp. 3505–3512.

Wetter, Michael et al. (2014). "Modelica Buildings library". In: *Journal of Building Performance Simulation* 7.4, pp. 253–270. DOI: 10.1080/19401493.2013.765506.

Zimmer, Dirk (2020). "Robust object-oriented formulation of directed thermofluid stream networks". In: *Mathematical and Computer Modelling of Dynamical Systems* 26.3, pp. 204–233. DOI: 10.1080/13873954.2020.1757726.

Zimmer, Dirk, Michael Meißner, and Niels Weber (2022). "The DLR ThermoFluid Stream Library". In: *Electronics* 11.22. ISSN: 2079-9292. DOI: 10.3390/electronics11223790.